Satellite and Ocean Data Reveal Marked Increase in Earth's Heating Rate

Norman G. Loeb[1*], Gregory C. Johnson[2], Tyler J. Thorsen[1], John M. Lyman[2,3], Fred G. Rose[4], and Seiji Kato[1]

[1]NASA Langley Research Center, Hampton, VA 23681, USA.

[2]NOAA/Pacific Marine Environmental Laboratory, Seattle, WA, USA

[3]Joint Institute for Marine and Atmospheric Research, University of Hawaii at Manoa, Honolulu, HI, USA

[4]Science Systems and Applications, Inc., Hampton, VA, USA

Key Points

- Satellite and in situ observations independently show an approximate doubling of Earth's Energy Imbalance (EEI) from mid-2005 to mid-2019
- Anthropogenic forcing, internal variability, and climate feedbacks all contribute to the positive trend in EEI
- Marked decreases in clouds and sea-ice and increases in trace gases and water vapor combine to increase the rate of planetary heat uptake

* Corresponding Author: Norman G. Loeb, norman.g.loeb@nasa.gov; NASA Langley Research Center, Hampton, VA 21 Langley Boulevard, Hampton, VA 23681

This article has been accepted for publication and undergone full peer review but has not been through the copyediting, typesetting, pagination and proofreading process, which may lead to differences between this version and the Version of Record. Please cite this article as doi: 10.1029/2021GL093047.

Abstract

Earth's Energy Imbalance (EEI) is a relatively small (presently ~0.3%) difference between global mean solar radiation absorbed and thermal infrared radiation emitted to space. EEI is set by natural and anthropogenic climate forcings and the climate system's response to those forcings. It is also influenced by internal variations within the climate system. Most of EEI warms the ocean; the remainder heats the land, melts ice, and warms the atmosphere. We show that independent satellite and in situ observations each yield statistically indistinguishable decadal increases in EEI from mid-2005 to mid-2019 of 0.50±0.47 W m^{-2} $decade^{-1}$ (5%-95% confidence interval). This trend is primarily due to an increase in absorbed solar radiation associated with decreased reflection by clouds and sea-ice and a decrease in outgoing longwave radiation (OLR) due to increases in trace gases and water vapor. These changes combined exceed a positive trend in OLR due to increasing global mean temperatures.

Plain Language Summary

Climate is determined by how much of the sun's energy the Earth absorbs and how much energy Earth sheds through emission of thermal infrared radiation. Their sum determines whether Earth heats up or cools down. Continued increases in concentrations of well-mixed greenhouse gasses in the atmosphere and the long time-scales time required for the ocean, cryosphere, and land to come to thermal equilibrium with those increases result in a net gain of energy, hence warming, on Earth. Most of this excess energy (about 90%) warms the ocean, with the remainder heating the land, melting snow and ice, and warming the atmosphere. Here we compare satellite observations of the net radiant energy absorbed by Earth with a global array of measurements used to determine heating within the ocean, land and atmosphere, and melting of snow and ice. We show that these two independent approaches yield a decadal increase in the rate of energy uptake by Earth from

mid-2005 through mid-2019, which we attribute to decreased reflection of energy back into space by clouds and sea-ice and increases in well-mixed greenhouse gases and water vapor.

1. Introduction

Increasing well-mixed greenhouse gases (WMGG) have led to an imbalance between how much solar radiant energy is absorbed by Earth and how much thermal infrared radiation is emitted to space. This net radiation imbalance, also referred to as Earth's energy imbalance (EEI), has led to increased global mean temperature, sea level rise, increased heating within the ocean, and melting of snow and sea ice (IPCC, 2013). In addition to anthropogenic radiative forcing by WMGG, EEI is influenced by aerosol emissions and land use change as well as by natural forcings associated with volcanic emissions and variations in solar irradiance. As the climate system responds to warming, changes in clouds, water vapor, surface albedo and temperature further alter EEI. These properties also respond to internal variations in the climate system occurring over a range of timescales, causing additional EEI variability. Examples of internal variations include weather events, which vary from days to weeks, El-Niño Southern Oscillation (ENSO) events (Philander, 1983), which vary on interannual timescales, and the Pacific Decadal Oscillation (PDO; Mantua et al. 1997), which varies on decadal timescales.

Since ~90% of the excess energy associated with EEI is stored in the ocean (von Schuckmann et al., 2020), fluctuations in Earth's top-of-atmosphere (TOA) net radiation and the ocean's heating rate should be in phase with one another (Palmer et al., 2011). Indeed, prior comparisons of EEI variations derived from in situ measurements after 2005 and satellite observations of Earth's net radiation track one another at interannual timescales (Johnson et al., 2016). More recently, analyses of ocean temperature data have indicated that the rate of ocean heating has been steadily increasing (von Schuckmann et al., 2020), but a direct comparison with satellite observations is lacking. In addition, sea level rise from 1993–2017 has exhibited a statistically significant acceleration (Nerem et al., 2018). However, acceleration of melting ice on

land accounts for the majority of sea level rise acceleration in recent decades, leaving less than 10% of the sea level acceleration signal attributed to increasing rates of ocean warming (Nerem et al., 2018).

In this study, we perform a direct comparison between variations in EEI inferred from the Clouds and the Earth's Radiant Energy System (CERES) and an in situ estimate of the observed ocean heat uptake over 0–2000 m combined with published estimates of energy uptake by the deeper ocean, lithosphere, cryosphere, and atmosphere. This comparison is made using annual estimates centered on mid-2005 (the year the Argo array of profiling floats achieved sparse near-global coverage) through mid-2019. Of particular interest are how consistently these two observing systems capture interannual variations and the trend in EEI. This is followed by a partial radiative perturbation (PRP) analysis using additional data sources in order to identify what properties of the climate system are contributing to the observed trend in EEI.

2. Data and Methods

2.1 Satellite Data

We use observational data from the CERES Energy Balanced and Filled (EBAF) Ed4.1 product (Loeb et al., 2018a, Kato et al., 2018). EBAF provides monthly mean TOA and surface shortwave (SW), longwave (LW) and net radiative fluxes on a 1°×1° grid along with imager-derived cloud properties. Here we only consider the TOA fluxes derived from CERES SW and LW radiance measurements and solar irradiance measurements. Absorbed solar radiation is determined from the difference between spatially and temporally averaged monthly solar irradiances and reflected SW fluxes. The solar irradiances are determined from time-varying instantaneous total solar irradiance measurements from various sources (Loeb et al., 2018a). In our comparisons with in situ EEI, we consider the period 01/2005-12/2019.

As noted in detail in Loeb et al. (2018a), EEI is a small (~0.15%) residual of much larger radiative fluxes that are on the order of 340 W m^{-2}. Satellite incoming and outgoing radiative fluxes are presently not at the level of accuracy required to resolve such a small difference in an absolute sense. However, satellite EEI are highly precise as the instruments are very stable. We thus adjust the satellite EEI to the in situ value by applying an offset to the satellite EEI such that its mean value over the 15-year period considered in this study is consistent with the mean in situ value. Use of this offset to anchor the satellite EEI to the in situ EEI does not affect the trends of either time series nor the correlation between them. Year-to-year variations and long-term trends in EEI from the satellite data are completely independent of those from the in situ data.

2.2 In Situ Data

An in situ estimate of planetary heat uptake for mid-2005 to mid-2019 is derived by an inventory of the rates of changes of energy stored in all components of the climate system. The primary contribution is from differences of overlapping annual 0–2000 m ocean heat content anomalies estimated at 6-monthly intervals from Argo float profiles. For example, the ocean heating rate estimate centered at mid-2005 is the estimate of ocean heat content anomaly for July 2005 to June 2006 minus that for July 2004 to June 2005.

The net heat uptake rate is estimated to be 0.77±0.06 W m^{-2} from mid-2005 to mid-2019. This rate is the sum of energy uptake rates of 0.62±0.05 W m^{-2} from the estimates in the ocean from 0–2000 m at 6-monthly intervals centered from mid-2005 through mid-2019, 0.062±0.038 W m^{-2} from May 1992 to June 2011 in the deeper ocean (Johnson et al., 2019), 0.037±0.004 W m^{-2} from mid-2005 to mid-2018 in the land, 0.031±0.006 W m^{-2} from mid-2005 to mid-2016 by melting ice, and 0.014±0.009 W m^{-2} from mid-2005 to mid-2018 by a warmer and moister atmosphere (von Schuckmann et al., 2020).

To determine year-to-year changes in planetary uptake, the 0–2000 m ocean heat uptake is from an estimate that uses local correlations between sea-surface height and ocean heat content anomalies to employ satellite altimetry data as a first guess at ocean heat content where (or when) in situ temperature data are sparse (Willis et al., 2003). For the period of study here, the fraction of the 0–2000 m ocean volume for which the first-guess estimate from the sea level and its correlation to ocean heat content is used in the absence of in situ ocean heat content data decreases from 23% for 2005 to about 8% after 2017 (following the methodology of Lyman and Johnson, 2014).

2.3 Partial Radiative Perturbation Analysis

The PRP method (Wetherald and Manabe, 1988) provides a means of determining anomalies in TOA radiation associated with individual variables. Here we use the PRP method as implemented in Thorsen et al. (2018) to identify the variables that drive any observed trends in global and regional TOA fluxes.

For non-cloud contributions, the effect on the flux (δF) due to some perturbation Δx of variable x is computed using a centered finite difference by averaging the backward finite difference:

$$\delta F^{b}_{\Delta x,M} = F(x, y_1, \ldots, y_N) - F(x - \Delta x, y_1, \ldots, y_N) \quad (1)$$

with the forward finite difference:

$$\delta F^{f}_{\Delta x,M} = F(x + \Delta x, y_1, \ldots, y_N) - F(x, y_1, \ldots, y_N) \quad (2)$$

where x, y_1,…,y_N are gridded monthly mean input variables to radiative transfer model calculations, and Δx, Δy_1, …, Δy_N are gridded deseasonalized monthly mean anomalies of the input variables, and *F* is the flux calculated using the NASA Langley Fu–Liou radiative transfer model (Rose et al., 2013). Deseasonalized monthly mean anomalies are obtained from the

difference between the monthly mean of a variable and its corresponding monthly climatology, determined by averaging all years of the same month. Input variables include skin temperature, profiles of temperature and water vapor, surface albedo, aerosols, trace gases (ozone, carbon dioxide, methane, nitrous oxide, CFC-11, CFC-12, and HCFC-22), and incoming solar irradiance. The input variables are those used in the surface flux calculations in the CERES EBAF Ed4.1 (Kato et al., 2018) consisting of adjusted input values provided in the CERES SYN1deg Ed4.1 product that are "tuned" to force a match between computed and observed EBAF monthly mean all-sky and clear-sky TOA fluxes through an objective containment algorithm (Rose et al., 2013; Kato et al. 2018). To determine cloud contributions, the approach of Soden et al. (2008) is used:

$$\delta F_{\Delta C} = \Delta CRE - \sum_i \left[\delta F_{\Delta x_i} - \delta F^o_{\Delta x_i}\right] \quad (2)$$

where ΔCRE is the anomaly in cloud radiative effect (CRE) from EBAF Ed4.1 observations, $\delta F_{\Delta x_i}$ is the all-sky flux perturbation due to an anomaly in variable x_i, and $F^o_{\Delta x_i}$ is the clear-sky flux perturbation due to an anomaly in variable x_i. Based upon direct comparisons between trends determined from CERES Terra and CERES Aqua monthly CRE anomalies for 09/2002-03/2020, we estimate the trend uncertainty in CRE due to instrument drift to be < 0.085 W m^{-2} $decade^{-1}$, which is a factor of 5 smaller than the trend uncertainty associated with CRE internal variability.

As described in more detail in Thorsen et al. (2018), skin temperature, surface pressure, and profiles of temperature, water vapor, and ozone are from the Goddard Earth Observing System (GEOS), version 5.4.1, reanalysis (Rienecker et al., 2008) or the Atmospheric Infrared Sounder (AIRS), version 6 level 3, standard product (Chahine et al., 2006; Tian et al., 2013). Carbon dioxide concentrations are obtained from the AIRS, version 5 level 3, carbon dioxide product (Chahine et al., 2005). Other trace gases are obtained from NOAA Earth System Research Laboratory (ESRL) Global Monitoring Division (Dlugokencky et al., 2009; Conway et al., 1994). Aerosol optical

depths (at 0.55 μm) and vertical distributions of seven aerosol types are from the Model of Atmospheric Transport and Chemistry (MATCH) Moderate Resolution Imaging Spectroradiometer (MODIS) aerosol assimilation product (Collins et al., 2001). Spectral surface albedos are determined using surface-type-based lookup tables (Jin et al., 2004; Rutan et al., 2009) for the spectral shapes that are scaled by the broadband surface albedo determined from the CERES surface albedo history (SAH) map (Rutan et al., 2009).

3. Results

3.1 Changes in Net TOA flux and Energy Uptake

We previously estimated, from in situ annual estimates of energy uptake by Earth's climate system, the EEI at 0.70±0.10 W m^{-2} (expressed here in terms of average heat uptake applied over Earth's surface area with 5–95% confidence intervals) from mid-2005 to mid-2015 (Johnson et al., 2016). We noted a 0.78 correlation between 0-1800 m year-to-year variations in ocean heating rate and satellite-based EEI from CERES. As detailed in section 2.2, here we update our calculations, extend them to 2000 m, and find a net heat uptake rate of 0.77±0.06 W m^{-2} from mid-2005 to mid-2019 (Fig. 1). With the longer time-series, the rate has increased, and the uncertainty has reduced slightly. The correlation between year-to-year rates of a global 0–2000 m ocean heat uptake and CERES EEI is 0.70 for the mid-2005 to mid-2019 estimates. An F-test for equality of two variances indicates that we cannot reject the null hypothesis that the sample variances of the in situ and satellite EEI datasets are equal at the 0.05 significance level.

A striking new result is that from the mid-2005 to mid-2019 estimates the trend of the energy flux for 0–2000 m ocean heat content anomaly (OHCA) is 0.43±0.40 W m^{-2} $decade^{-1}$, and the trend for the net CERES TOA energy flux is 0.50±0.47 W m^{-2} $decade^{-1}$ over that same time period (Fig. 1, dashed lines). The trend in the difference between the CERES and in-situ data is

0.068±0.29 W m^{-2} $decade^{-1}$. Trends are determined using least squares linear regression and uncertainties in the trends correspond to 5-95% confidence intervals, accounting for autocorrelation in the data following the methodology of Santer et al. (2000). This remarkable increase in EEI is consistent between these two completely independent observational estimates. The linear trend of CERES implies a net EEI of 0.42±0.48 W m^{-2} in mid-2005 and 1.12±0.48 W m^{-2} in mid-2019. The in situ estimates yield a statistically indistinguishable result.

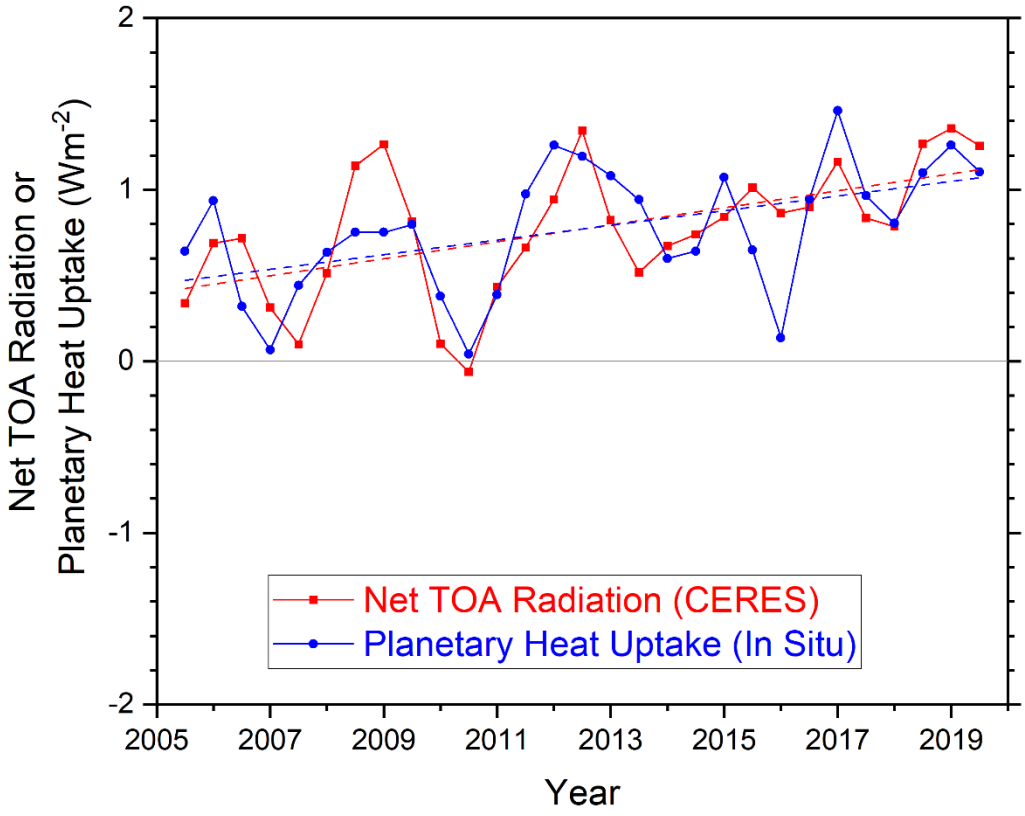

Figure 1 Comparison of overlapping one-year estimates at 6-month intervals of net top-of-the-atmosphere annual energy flux from the CERES EBAF Ed4.1 product (solid red line) and an in situ observational estimate of uptake of energy by Earth climate system (solid blue line). Dashed lines correspond to least squares linear regression fits to the data.

3.2 Attribution of EEI Trends

We consider CERES TOA EEI trends for 09/2002-03/2020 and examine the underlying contributions from different atmospheric and surface variables available over that time period.

Trends are determined from a least-squares regression fit to deseasonalized monthly anomalies with uncertainties given as 5%-95% confidence intervals.

For this period, the observations show a trend in net downward radiation of 0.41±0.22 W m^{-2} $decade^{-1}$ that is the result of the sum of a 0.65±0.17 W m^{-2} $decade^{-1}$ trend in absorbed solar radiation (ASR) and a –0.24±0.13 W m^{-2} $decade^{-1}$ trend in downward radiation due to an increase in OLR (Figs. 2a-c). TOA fluxes are defined positive downwards so that a positive anomaly/trend corresponds to a heat gain and a negative anomaly corresponds to a heat loss. As such, emitted thermal radiation (ETR) is defined positive downward and is therefore equal to –OLR. The TOA anomalies are also consistent across CERES instruments on different satellite platforms (Loeb et al., 2018b). The ASR trend cannot be explained by changes in incoming solar radiation, as the trend in incoming solar flux is negligible (–0.053 W m^{-2} $decade^{-1}$).

Our PRP results (Fig. 2d-f) consider contributions from changes in clouds, water vapor, combined contributions from trace gases and solar irradiance (labled as "Other"), surface albedo, aerosols, and combined contributions from skin temperature and profiles of temperature (labeled as "Temp"). We note that the aerosol contributions to TOA flux variations only include aerosol-radiation interactions. Any change in TOA radiation due to aerosol-cloud interactions is implicitly included here as part of the cloud contribution. Most of the ASR trend is associated with cloud and surface albedo changes (Fig. 2d), which account for 62% and 27% of the ASR trend, respectively. Increasing global mean surface temperatures and cloud changes during the past two decades have contributed to an increase in thermal infrared emission to space, which is partly compensated for by increases in water vapor and trace gases (Fig. 2e). The overall trend in net radiation is a result of the sum of positive trends in contributions from clouds, water vapor, trace gases, surface albedo, and aerosols, which exceeds the negative contribution from temperature (Fig. 2f).

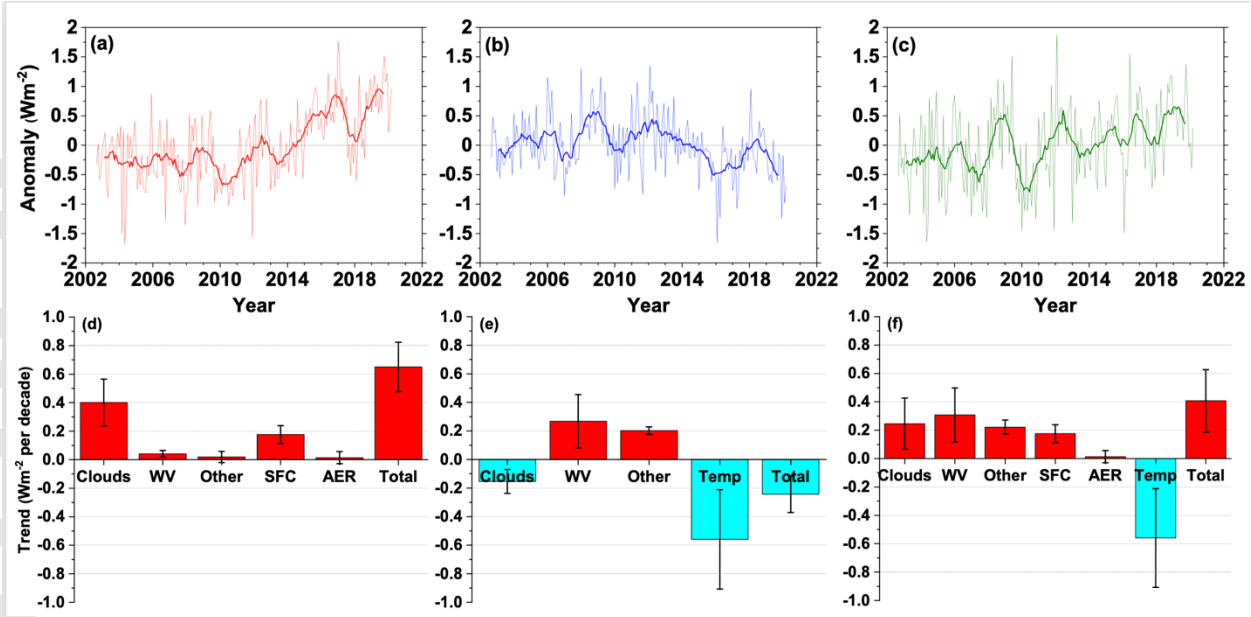

Figure 2 Global mean TOA flux anomalies and trends. Anomalies in (a) ASR, (b) ETR and (c) Net for 2002/09-2020/03. Thin lines correspond to monthly anomalies, thick lines are 12-month running averages. Trends in (d) ASR, (e) ETR and (f) Net associated with contributions from changes in clouds, water vapor (WV), combined contributions from trace gases and solar irradiance (labeled as "Other"), surface albedo (SFC), aerosols (AER) and combined contributions from skin temperature and profiles of temperature ("Temp"). "Total" corresponds to the sum of the individual contributions. Error bars correspond to 5-95% confidence intervals determined using the methodology in Santer et al. (2000). Positive anomalies and trends correspond to heat gain, and negative to loss. ETR is defined positive downwards and is thus equal to –OLR.

Regional trends in net radiation attributable to changes in clouds are strongly positive along the east Pacific Ocean, while more modest positive trends occur off of the U.S. east coast and over the Indian, Southern, and central equatorial Pacific Oceans (Fig. 3a). Net TOA flux trends due to surface albedo are greatest in areas of snow and sea-ice (Fig. 3b), where significant declines in coverage have been observed in recent decades (Alexander et al., 2013). Trends in net TOA flux due to temperature changes are negative almost everywhere (Fig. 3c), while water vapor trends are predominantly positive, particularly over land (Fig. 3e). Contributions from trace gases are uniform everywhere (Fig. 3d), whereas trends associated with aerosol changes are positive over China, USA and Europe, and negative over India (Fig. 3f).

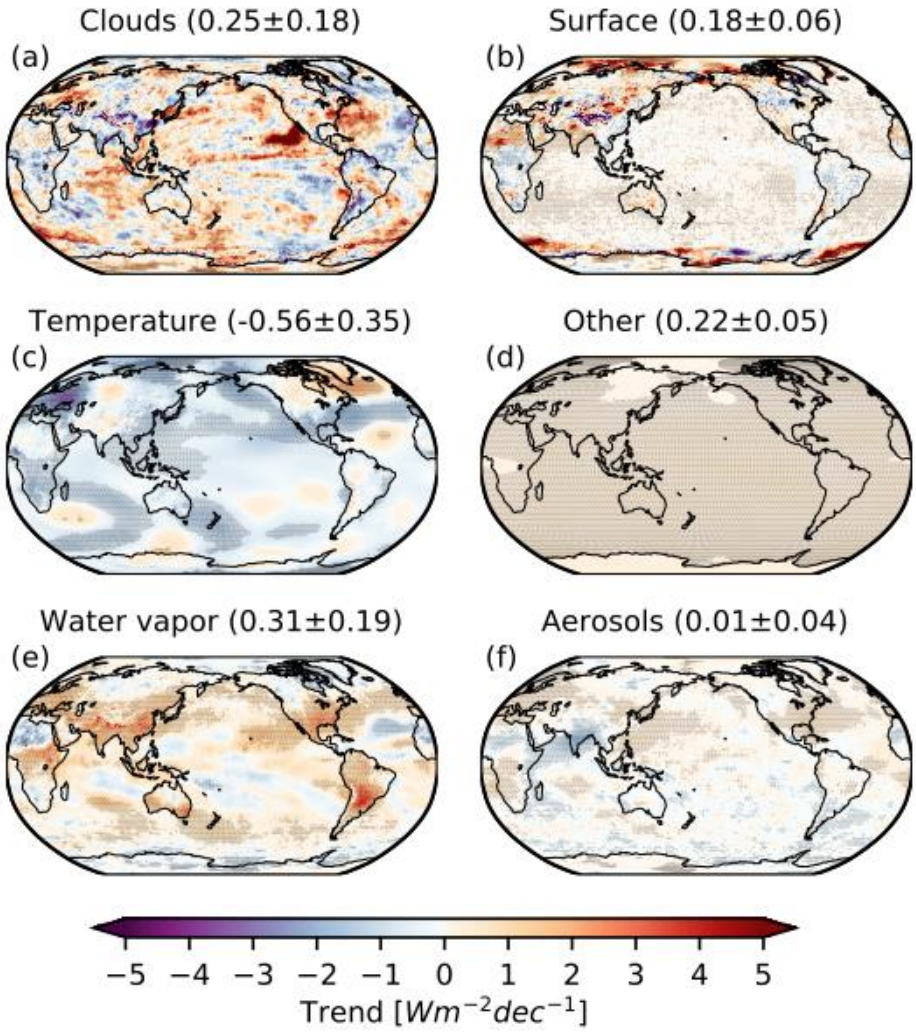

Figure 3 Attribution of CERES net TOA flux trends for 2002/09-2020/03. Shown are trends due to changes in (a) clouds, (b) surface, (c) temperature, (d) combined contributions from trace gases and solar irradiance (labeled as "Other"), (e) water vapor, and (f) aerosols. Positive trends correspond to heat gain and negative to loss. Stippled areas fall outside the 5%-95% confidence interval. Numbers in parentheses correspond to global trends and 5%-95% confidence intervals in W m^{-2} $decade^{-1}$.

An additional factor that explains the trend in net TOA flux is the shift from a negative to a positive PDO index in 2014 (Fig. 4a). The PDO is a large-scale climate pattern associated with substantial shifts in sea-surface temperatures (SSTs) and clouds and has been previously linked to variability in the EEI as estimated at the TOA by satellite data (Loeb et al., 2018b). Following the shift in the sign of the PDO index in 2014, the Niño3.4 index peaked during the winter of 2015/2016, reflecting a major El Niño event (Fig. 4b). SSTs started to rise in 2012 and have

remained above average through 2020 (Fig. 4c). Variations in SST closely track both the PDO and Niño3.4 indices, with correlation coefficients 0.80 and 0.72, respectively. In the positive phase of the PDO, SST increases are pronounced over the eastern Pacific Ocean, which causes a decrease in low cloud amount and an increase in ASR along the eastern Pacific Ocean (Loeb et al., 2018b). After 2014, the ASR trend shows a factor of 4 increase over that prior to 2014. An increase in thermal infrared emission to space slightly offsets the increase in ASR, so that the trend in net flux after 2014 is reduced to 2.5 times that prior to 2014.

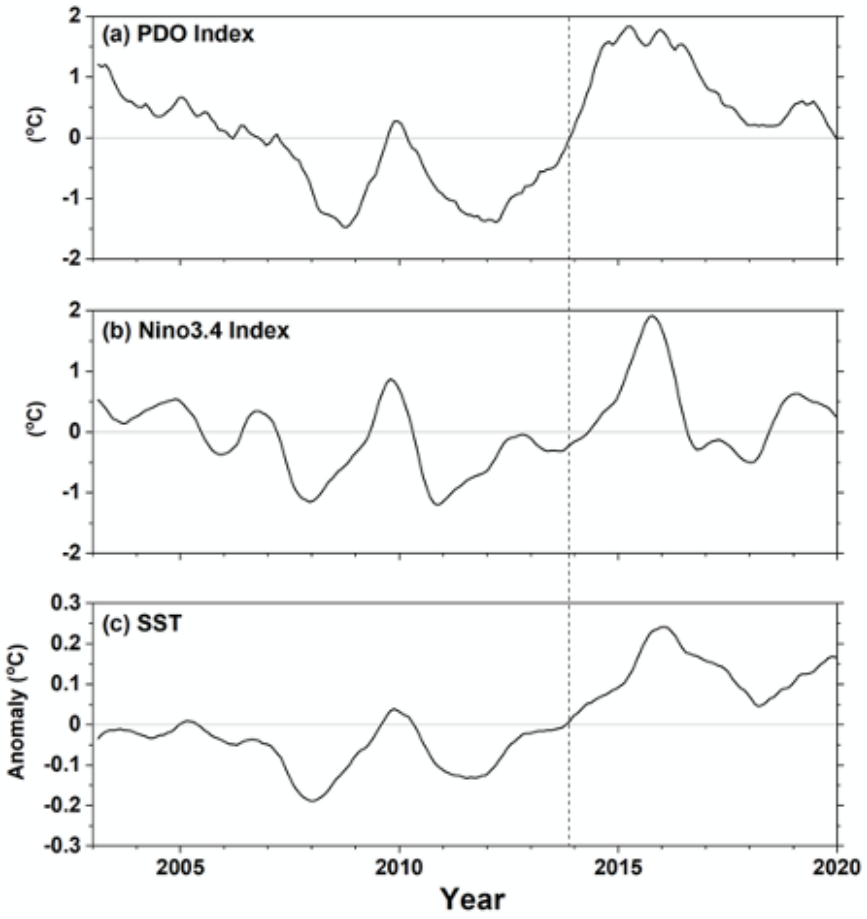

Figure 4 Time series of PDO, Niño3.4 and SST. (a) PDO Index, (b) Niño3.4 Index and (c) anomalies in SST. Vertical dashed line corresponds to shift in sign of PDO index from negative to positive in 2014.

4. Conclusions

The excellent agreement between satellite and in situ trends in EEI obtained in this study demonstrates the benefits of having independent satellite TOA radiation observations and ocean heat content measurements for tracking changes in EEI. That both produce nearly identical results provides confidence that the trend towards an increased EEI reported here is robust, since it is unlikely to be due to artifacts in both observing systems. The positive trend in EEI is a result of combined changes in clouds, water vapor, trace gases, surface albedo, and aerosols, which exceed a negative contribution from increasing global mean temperatures. At global scale, the aerosol contribution is small compared to other contributions. This may be because only aerosol direct radiative effects are explicitly calculated as part of the aerosol contribution. Aerosol indirect effects are implicitly included as part of the cloud contribution to EEI—quantifying the aerosol indirect effect would require model simulations that can be run with and without aerosol-cloud interactions.

Because EEI is such a fundamental property of the climate system, the implications of an increasing EEI trend are far reaching. A positive EEI is manifested as 'symptoms' such as global temperature rise, increased ocean warming, sea level rise, and intensification of the hydrological cycle (von Schuckmann et al., 2016). We can therefore expect even greater changes in climate in the coming decades if internal variability associated with the PDO remains the same. If the PDO were to reverse in the future, that reversal would likely act to decrease the rate of heat uptake. Further modeling studies are needed to fully understand the impact of the increasing trend in EEI on global and regional surface temperature, sea level rise, and changes to the hydrological cycle.

Acknowledgements

We thank the CERES science, algorithm, and data management teams and the NASA Science Mission Directorate for supporting this research. G.C.J. and J.M.L. are supported by the National Oceanic and Atmospheric Administration (NOAA) Global Ocean Monitoring and

Observations Program and NOAA Research. This is PMEL Contribution 5196 and JIMAR contribution number 20-400. CERES_EBAF Ed4.1 was obtained from the CERES ordering page at http://ceres.larc.nasa.gov/order_data.php. PDO index data was obtained from https://climexp.knmi.nl/data/ipdo.dat and accessed on November 3, 2020. Nino3.4 index data is from ESRL/NOAA obtained from https://psl.noaa.gov/data/correlation/nina34.data. Ocean heat content anomaly data used to determine the in situ EEI was obtained from https://oceans.pmel.noaa.gov. Partial radiative perturbation anomalies were obtained from https://ceres.larc.nasa.gov/ceres-prp-anomalies.php. We also thank Drs. Bjorn Stevens and George Datseris for their helpful comments.

References

Alexander, L. V. & and Co-Authors. Summary for Policymakers. in Climate Change 2013: The Physical Science Basis. Contribution of Working Group I to the Fifth Assessment Report of the Intergovernmental Panel on Climate Change 3–29 (Cambridge University Press, 2013).

Chahine, M., Barnet, C., Olsen, E. T., Chen, L. & Maddy, E. (2005). On the determination of atmospheric minor gases by the method of vanishing partial derivatives with application to CO2. Geophysical Research Letters 32.

Chahine, M. et al. (2006). AIRS: Improving weather forecasting and providing new data on greenhouse gases. Bulletin of the American Meteorological Society 87, 911–926.

Collins, W. D., Rasch, P. J. Eaton, B. E., Khattatov, B. V., Lamarque, J.-F., & Zender, C. S. (2001). Simulating aerosols using a chemical transport model with assimilation of satellite aerosol retrievals: Methodology for INDOEX. J. Geophys. Res., 106, 7313–7336, https://doi.org/10.1029/2000JD900507.

Conway, T. J., Tans, P. P., Waterman, L. S., Thoning, K. W., Kitzis, D. R., Masarie, K. A., & Zhang, N. (1994). Evidence for interannual variability of the carbon cycle from the National Oceanic and Atmospheric Administration/Climate Monitoring and Diagnostics Laboratory Global Air Sampling Network. J. Geophys. Res., 99, 22 831–22 855, https://doi.org/ 10.1029/94JD01951.

Dlugokencky, E. J. et al. (2009). Observational constraints on recent increases in the atmospheric CH4 burden. Geophys. Res. Lett. Geophysical Research Letters, 36, L18803, https://doi.org/10.1029/2009GL039780.

IPCC, 2013: Summary for Policymakers. In: Climate Change 2013: The Physical Science Basis. Contribution of Working Group I to the Fifth Assessment Report of the Intergovernmental Panel on Climate Change [Stocker, T.F., D. Qin, G.-K. Plattner, M. Tignor, S.K. Allen, J. Boschung, A. Nauels, Y. Xia, V. Bex and P.M. Midgley (eds.)]. Cambridge University Press, Cambridge, United Kingdom and New York, NY, USA.

Jin, Z., Charlock, T. P., Smith, W. L. & Rutledge, K. (2004). A parameterization of ocean surface albedo. Geophysical Research Letters 31, L22301, https://doi.org/10.1029/2004GL021180.

Johnson, G. C., Lyman, J. M. & Loeb, N. G. (2016). Improving estimates of Earth's energy imbalance. Nature Climate Change 6, 639–640.

Johnson, G. C. et al. (2019). Ocean heat content in the State of the Climate in 2018. Bull. Am. Meteorol. Soc. 100, S74–S76.

Kato, S. et al. (2018). Surface Irradiances of Edition 4.0 Clouds and the Earth's Radiant Energy System (CERES) Energy Balanced and Filled (EBAF) Data Product. J. Climate 31, 4501–4527.

Loeb, N. G., Doelling, D. R., Wang, H., Su, W., Nguyen, C., Corbett, J. G., et al. (2018a). Clouds and the Earth's Radiant Energy System (CERES) energy balanced and filled (EBAF) top-of-atmosphere (TOA) Edition 4.0 data product. Journal of Climate, 31, 895–918. https://doi.org/10.1175/JCLI-D-17-0208.1.

Loeb, N. G., Thorsen, T. J., Norris, J. R., Wang, H., & Su, W. (2018b). Changes in earth's energy budget during and after the "pause" in global warming: An observational perspective. MDPI Climate, 6, 62. https://doi.org/10.3390/cli6030062.

Lyman, J. M. and G. C. Johnson. 2014. Estimating global ocean heat content changes in the upper 1800 m since 1950 and the influence of climatology choice. Journal of Climate, 27, 1946-1958, doi:10.1175/ JCLI-D-12-00752.1.

Mantua, N., Hare, S. R., Zhang, Y., Wallace, J. M. & Francis, R. C. (1997). A Pacific interdecadal climate oscillation with impacts on salmon production. Bulletin of the American Meteorological Society 78, 1069–1079.

Nerem, R. S. et al. (2018). Climate-change-driven accelerated sea-level rise detected in the altimeter era. Proceedings of the National Academy of Sciences of the United States of America 115, 2022–2025.

Palmer, M. D., McNeall, D. J. & Dunstone, N. J. (2011): Importance of the deep ocean for estimating decadal changes in Earth's radiation balance. Geophys. Res. Lett. 38, L13707.

Philander, S. (1983). El Niño Southern Oscillation phenomena. Nature 302, 295–301.

Rienecker, M. M. et al. (2008). The GEOS-5 Data Assimilation System—Documentation of versions 5.0.1, 5.1.0, and 5.2.0. 97 http://gmao.gsfc.nasa.gov/pubs/docs/ Rienecker369.pdf.

Rose, F. G., Rutan, D. A., Charlock, T., Smith, G. L. & Kato, S. (2013). An Algorithm for the Constraining of Radiative Transfer Calculations to CERES-Observed Broadband Top-of-Atmosphere Irradiance. Journal of Atmospheric and Oceanic Technology 30, 1091–1106.

Rutan, D. et al. (2009). Development and assessment of broadband surface albedo from Clouds and the Earth's Radiant Energy System Clouds and Radiation Swath data product. Journal of Geophysical Research 114.

Santer, B. D., T. M. L. Wigley, J. S. Boyle, D. J. Gaffen, J. J. Hnilo, D. Nychka, D. E. Parker, and K. E. Taylor, 2000: Statistical significance of trends and trend differences in layer-average atmospheric temperature time series. J. Geophys. Res., 105, 7337-7356.

Soden, B. J., Held, I. M., Colman, R., Shell, K. M., Kiehl, J. T., & Shields, C.A. (2008). Quantifying climate feedbacks using radiative kernels. J. Climate, 21, 3504–3520, https://doi.org/10.1175/2007JCLI2110.1.

Thorsen, T. J., Kato, S., Loeb, N. G. & Rose, F. G. (2018). Observation-based decomposition of radiative perturbations and radiative kernels. J. Climate 31, 10039–10058.

Tian, B. et al. (2013). Evaluating CMIP5 models using AIRS tropospheric air temperature and specific humidity climatology. J. Geophys. Res. Atmos. 118, 114–134.

Tian, B., Fetzer, E. J., Kahn, B. H., Teixeira, J., Manning, E., & Hearty, T. (2013). Evaluating CMIP5 models using AIRS tropospheric air temperature and specific humidity climatology. J. Geophys. Res. Atmos., 118, 114–134, https://doi.org/10.1029/2012JD018607.

von Schuckmann, K. et al. (2016). An imperative to monitor Earth's energy imbalance. Nature Climate Change 6, 138–144.

von Schuckmann, K. et al. (2020). Heat stored in the Earth system: where does the energy go? Earth Syst. Sci. Data 12, 2013–2041.

Wetherald, R. T., & Manabe, S., (1988). Cloud feedback processes in a general circulation model. J. Atmos. Sci., 45, 1397–1416, https://doi.org/10.1175/15200469(1988)045,1397:CFPIAG.2.0.CO;2.

Willis, J. K., Roemmich, D. & Cornuelle, B. (2003). Combining altimetric height with broadscale profile data to estimate steric height, heat storage, subsurface temperature, and sea-surface temperature variability. Journal of Geophysical Research: Oceans 108.